On the Electronic and Atomic Structures of Small Au_N^- ($N = 4-14$) Clusters: A Photoelectron Spectroscopy and Density-Functional Study

Hannu Häkkinen,* Bokwon Yoon, and Uzi Landman

School of Physics, Georgia Institute of Technology, Atlanta, Georgia 30332

Xi Li, Hua-Jin Zhai, and Lai-Sheng Wang

Department of Physics, Washington State University, 2710 University Drive, Richland, Washington 99352, and W. R. Wiley Environmental Molecular Sciences Laboratory, Pacific Northwest National Laboratory, MS K8-88, P.O. Box 999, Richland, Washington 99352

Received: May 23, 2003; In Final Form: June 24, 2003

We report a joint experimental and theoretical study of the electronic and atomic structures of small gold clusters with up to 14 atoms. Well-resolved photoelectron spectra were obtained for Au_N^- ($N = 1-14$) at several photon energies. Even−odd alternations were observed, where the even-sized clusters (except Au_{10}^-) exhibit an energy gap between the lowest binding energy peak and the rest of the spectrum, indicating that all the neutral even-sized clusters have closed shells. The Au_{10}^- spectrum reveals the existence of isomers, with the ground-state cluster exhibiting an extremely high electron binding energy. Evidence of multiple isomers was also observed in the spectra of $N = 4$, 8, 12, and 13. The structures of the gold cluster anions in the range $N = 4-14$ were investigated using first-principles simulations. A striking feature of the anionic clusters in this range is the occurrence of planar ground-state structures, which were predicted in earlier theoretical studies (Häkkinen, H.; et al. *Phys. Rev. Lett.* **2002**, *89*, 033401) and observed in ion-mobility experiments (Furche, F.; et al. *J. Chem. Phys.* **2002**, *117*, 6982) and the existence of close-lying isomers. The calculated electron detachment energies and density of states were compared with the measured data, which confirmed the ground-state structures of the anions. It is found that the main isomers observed experimentally indeed consist of planar clusters up to Au_{12}^-, whereas for Au_{13}^- and Au_{14}^- the theoretical results from three-dimensional isomers agree better with the experiment, providing further support for the 2D to 3D structural transition at Au_{12}^-, as concluded from previous ion mobility experiments. We also find that small neutral clusters exhibit a tendency to form two-dimensional structures up to a size of 13 atoms.

I. Introduction

The recent surge of research activity in the area of the physical and chemical properties of gold clusters and nanoparticles is motivated by their potential applications as building blocks for functional nanostructured materials, electronic devices, and nanocatalysts.[1−27] An added interest was created by the most recent experimental and theoretical discoveries of large (up to about 12 atoms) planar gas-phase anionic gold clusters.[17,18] The occurrence of planar metal clusters of this size is unprecedented, and their stability was explained by, and attributed to,[18] strong relativistic bonding effects[28] in gold that reduce the s−d energy gap, thus inducing hybridization of the atomic 5d−6s levels and causing overlap of the 5d shells of neighboring atoms in the cluster.

We report here a systematic combined high-resolution photoelectron spectroscopy and density-functional investigation of the atomic and electronic structure of gold cluster anions Au_N^- with $N = 1-14$. This study is complementary in many ways to the ones reported previously. First, it provides photoelectron spectra (PES) with much better resolution than the previous works[2,3] enabling identification of several new important features due to isomers in the cluster beam. Second, our density-functional calculations extend the range of those reported by us before,[12,18] including a critical examination of several cluster isomers for each cluster size. Finally, comparison of our calculated results with the experiments reported here allows us to assign the probable ground-state structures and the important isomers existing in the cluster beam, providing the basic structural information for future studies of the physics and chemistry of these systems.[18]

The paper is organized as follows. Brief descriptions of the experimental and theoretical methods used in this study are given in sections II and III. The experimental results are presented in section IV, and section V gives the theoretical results and a discussion of the comparison between the theoretical predictions and the measured data. We summarize our results in section VI.

II. Experimental Details

The experiments were performed using a magnetic-bottle photoelectron apparatus equipped with a laser vaporization cluster source.[29,30] A pure gold disk target was ablated by a pulsed laser beam (10 mJ/pulse at 532 nm). The laser-induced plasma was mixed with a helium carrier gas delivered by a pulsed valve at a backing pressure of 10 atm. The clusters formed in the nozzle were entrained with the carrier gas and

* Corresponding author. Current address: Department of Physics, FIN - 40014 University of Jyväskylä, Finland. E-mail: Hannu.Hakkinen@phys.jyu.fi.

10.1021/jp035437i CCC: $25.00
Published on Web 07/23/2003

underwent a supersonic expansion. After passing a skimmer, negatively charged gold clusters were extracted from the collimated cluster beam perpendicularly and subjected to a time-of-flight mass analysis. A given cluster of interest was mass-selected and decelerated before photodetachment by an ArF excimer laser (193 nm) or a Nd:YAG laser (266 and 355 nm). Photoelectrons were measured using a magnetic-bottle time-of-flight analyzer and calibrated by the known spectra of Au^- and Rh^-. Care was taken to produce relatively cold clusters, which are essential to yield highly resolved photoelectron spectra.[31,32] The experimental resolution ($\Delta E/E$) was ~2.5%, i.e., ~25 meV for 1 eV electrons.

III. Computational Methods

The electronic and geometric structures of the gold cluster anions were obtained through Born−Oppenheimer (BO) local spin-density-functional (LSD) molecular dynamics (MD) simulations (BO-LSD-MD)[33] employing norm-conserving scalar-relativistic pseudopotentials[34] for the $5d^{10}6s^1$ valence electrons of the gold atom, with self-consistent gradient corrections (PBE-GGA).[35] The Kohn−Sham (KS) orbitals were expanded in a plane-wave basis with a 62 Ry kinetic energy cutoff. This approach has been used by us in numerous occasions previously and its feasibility and accuracy for gold has been well documented.[12,14,18] The BO-LSD-MD method is particularly suited for studies of finite charged systems because it does not employ a supercell (periodic replication of the atoms), thus allowing for accurate determination of the total energy of both charged and neutral systems and the corresponding electron removal (detachment) energies. All the clusters were relaxed fully without any symmetry constraints. A large number of initial structural candidates were used, but here we report only the few energetically lowest-lying isomers for each size, which are important in interpreting the experimental data.

IV. Experimental Photoelectron Spectra

The photoelectron spectra for Au_N^- ($N = 1-14$) are shown in Figures 1 and 2 at 193 nm (6.424 eV) and 266 nm (4.661 eV), respectively. A few selected clusters with lower electron binding energies were also investigated at 355 nm (3. 496 eV), as shown in Figure 3, where only the threshold peak was observed in each case. The spectra were all highly resolved with numerous discrete electronic transitions up to the highest photon energy used (6.424 eV).

A. 193 nm Spectra. The current data at 193 nm are consistent with the previous data measured at 157 nm (ref 2) but are much better resolved. Our spectra for Au_2^- to Au_4^- at 193 nm were also consistent with a previous study at the same photon energy, except for the peak at 6.26 eV for Au_2^-, which was not observed in the previous work.[3] The most significant feature in the spectra is the even−odd alternation, where the even clusters show lower electron binding energies and a sizable energy gap (between the lowest-binding-energy peak and the rest of the spectrum), indicating that the neutral even-sized clusters are closed-shell electronic systems. The largest energy gap was observed in the spectrum of Au_6^-: 2.34 eV, which is in fact the largest among all the coinage metal clusters, even larger than the 1.8 eV gap recently found in the tetrahedral Au_{20}.[25]

However, the spectrum of Au_{10}^- represents a clear exception to the even−odd pattern. The weak signals in the lower binding energy range between 2.6 and 3.8 eV of the Au_{10}^- spectrum were actually due to weakly populated isomers. In fact, the vertical binding energy (VDE) of the main isomer of Au_{10}^- was measured to be 3.92 eV, higher than that of either Au_9^- (3.84 eV) or Au_{11}^- (3.80 eV). Minor isomers were also observed for other clusters, notably in the spectrum of Au_4^-, where two weak features were observed in the HOMO−LUMO gap region at VDEs of 3.41 and 3.76 eV. A very weak peak at 2.49 eV in the Au_4^- spectrum should also come from an isomer. In the spectra of Au_8^- and Au_{12}^-, the first peak showed a splitting, each with a shoulder on the higher energy side. The splitting is too large to be attributed to vibrational excitations and it is likely due to the presence of isomers with similar VDEs as the main isomers. The weak feature at the lowest energy side (3.76 eV) in the spectrum of Au_{13}^- is also indicative of a contribution from a minor isomer. As will be shown later, all the observed isomers are indeed born out from the accompanying theoretical calculations.

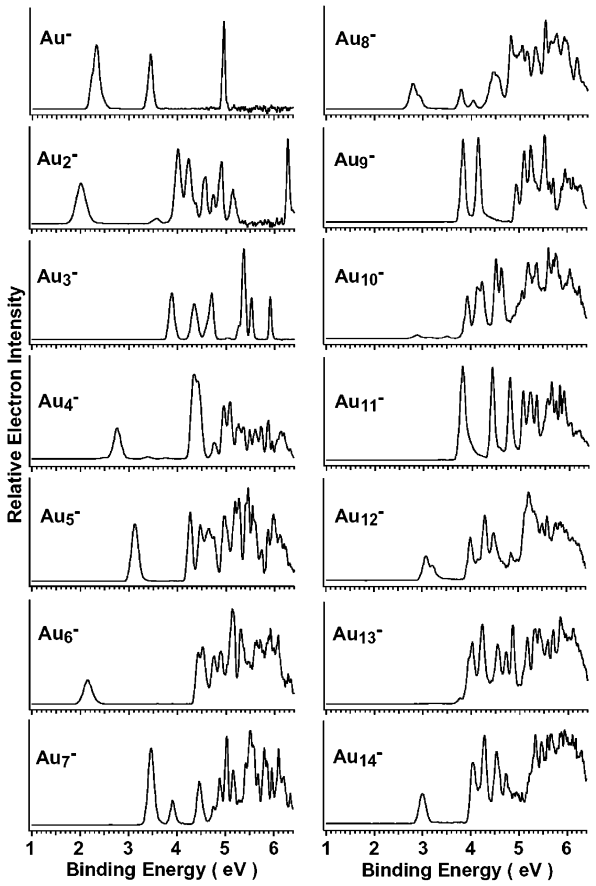

Figure 1. Photoelectron spectra of Au_N^- ($N = 1-14$) measured at 193 nm (6.424 eV).

B. 266 and 355 nm Spectra. The spectra at 266 nm were much better resolved for the low binding energy features accessible at this photon energy (Figure 2). In particular, the weak features attributed to anion isomers in the spectra of Au_4^-, Au_8^-, Au_{10}^-, Au_{12}^-, and Au_{13}^- can be seen more clearly. The spectrum of Au_3^- exhibited the most dramatic dependence on the photon energy: the relative intensities of the first two peaks (VDEs: 3.88 and 4.39 eV) were similar at 193 nm, but the relative intensity of the 4.39 eV peak was significantly reduced at 266 nm. The 3.88 eV peak of Au_3^- was extremely sharp, its width (40 meV fwhm) was close to the instrumental resolution, indicating that there is no geometry change between the anion and the neutral ground states for the gold trimer.

The spectra of other clusters did not display much photon energy dependence, except the surprising observation of continuous electron signals in the HOMO−LUMO gap region in the spectra of Au_{12}^- and Au_{14}^-. Similar signals were also observed as a higher binding energy tail in the spectra of Au_6^-

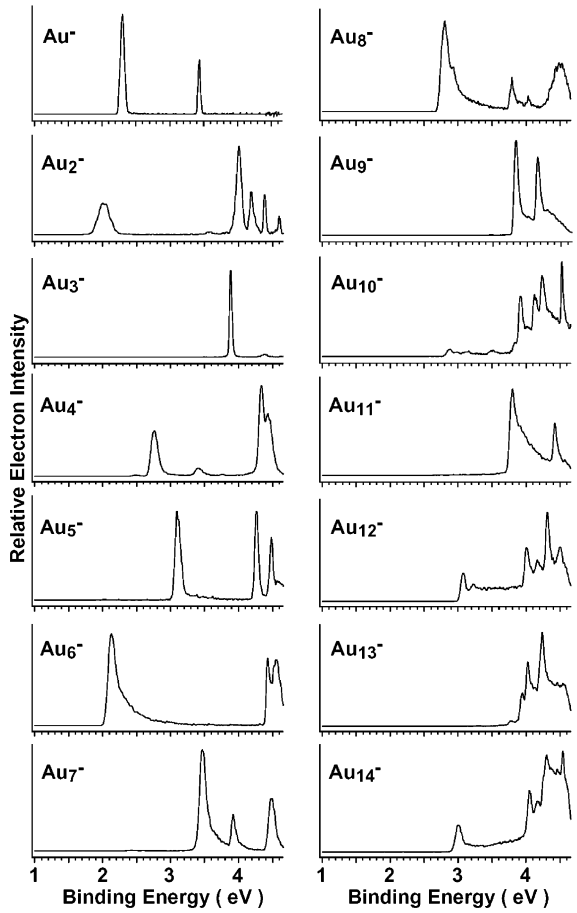

Figure 2. Photoelectron spectra of Au_N^- ($N = 1-14$) measured at 266 nm (4.661 eV).

and Au_8^-. To a lesser degree, the tails were also present in the 266 nm spectra of Au_7^-, Au_9^-, and Au_{11}^-. These signals seemed to be continuous and featureless; they were not due to contributions from isomers. These signals exhibited no photon flux dependence, but depended on the detachment photon energies because they were not observed in the 193 nm spectra. They appeared to be due to delayed detachment, analogous to delayed ionization observed for neutral clusters.[36] It seemed that the parent anion was capable of absorbing a photon to create a temporarily excited anion, which then autodetached. This absorption might be due to the plasma resonance of the anionic clusters. Plasma resonance has been observed in neutral and cationic alkali and coinage clusters,[37,38] though none has been reported for anionic clusters.

We only obtained spectra at 355 nm for a few selected clusters (Figure 3). We were particularly interested in resolving the splittings of the two features in the spectra of Au_8^- and Au_{12}^-. Unfortunately, the delayed detachment signals were sufficiently strong to wash out the weaker feature on the higher energy side. It turned out that these features were better observed in the 266 nm spectra (Figure 2). The second feature was observed to have VDEs of 2.93 and 3.22 eV, compared to the main feature at 2.79 and 3.06 eV for Au_8^- and Au_{12}^-, respectively.

C. Adiabatic and Vertical Detachment Energies. The VDEs for each cluster anion can be easily determined from the peak maximum in each spectrum. The adiabatic detachment energies (ADEs), which also represent the electron affinities (EAs) of the corresponding neutral clusters, were more difficult to measure without vibrational resolution. We estimated the ADEs by drawing a straight line at the leading edge of the ground-state feature and then adding a constant to the intersections with the binding energy axis to account for the instrumental resolution. Although this is an approximate procedure, we were able to obtain consistent ADEs from spectra taken at different photon energies, due to the relative sharp onset of the data. All the ADEs were determined from the 266 nm spectra or the 355 nm spectra, when available. More accurate ADEs were obtained in the lower photon energy spectra because of the better resolved features. The obtained ADEs and VDEs are listed in Table 1.

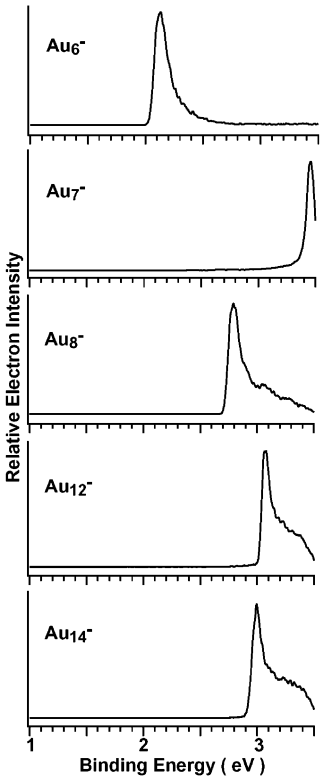

Figure 3. Photoelectron spectra of Au_N^- ($N = 6, 7, 8, 12, 14$) measured at 355 nm (3.496 eV).

V. Theoretical Results and Discussion

A. Low-Energy Structures and Detachment Energies. A number of optimized low-energy structures for Au_N^-, with $N = 4-14$, are shown in Figure 4 and their structural and energetic characteristics are summarized in Table 1. A striking feature in Figure 4 is the occurrence of energetically favorable *planar* structures up to Au_{14}^- (for clusters larger than Au_{10}^-, many low-lying 3D isomers appear but the ground-states predicted by DFT are still strictly planar). This phenomenon is unique to gold clusters and is related to strong relativistic effects in their bonding, which lead to enhanced s−d hybridization and d−d interaction, as was discussed recently by some of us.[18] Recent ion mobility experiments and related DFT calculations also yield support for large planar gold anions[17] up to about $N = 12$ (for $N = 12$ two distinct mobilities were detected and assigned to a coexistence of both planar and 3D structures).

Figure 5 shows the comparison of the calculated and measured VDEs. For most clusters, the theoretical ground-state VDE value (filled dot) is within 5−6% of the experimental result. For $N = 4$ and 14, the best agreement with experiment is obtained not for the ground-state structure, but rather for certain low-lying isomers. This indicates that even though the high resolution of the experimental PES data implies that the temperature of the cluster beam is low (in a previous study of anionic aluminum clusters in a similar setup the minimum

TABLE 1: Various Structural and Energetic Characteristics of Anionic Gold Clusters Au_N^- with $N = 4-14$[a]

	sym	crd	⟨*d*⟩ (Å)	Δ*E* (eV)	Δ*E* (K)	VDE^t (eV)	VDE^e (eV)	ADE^t (eV)	ADE^e (eV)	O^n
Au_2^-	$D_{\infty h}$	1	2.65	0	0	2.08	2.01(3)	2.02	1.92(4)	1
Au_3^-	$D_{\infty h}$	1.33	2.60	0	0	3.64	3.88(2)	3.64	3.88(2)	2
Au_4^-							2.75(3)		2.70(3)	
A 2D	C_{2h}	1.50	2.60	0	0	3.30		3.14		3
B 2D	C_{2v}	2.00	2.68	0.01	39	2.78		2.74		2
C 1D	$D_{\infty h}$	1.50	2.63	0.06	232	3.53		3.51		4
D 2D		2.50	2.73	0.10	386	2.64		2.56		1
Au_5^-							3.09(3)		3.06(3)	
A 2D	C_{2v}	2.80	2.73	0	0	3.09		3.06		1
B 2D	C_{2h}	1.60	2.60	0.31	800	4.11		3.96		2
C 1D	$D_{\infty h}$	1.60	2.62	0.57	1470	4.23		4.23		3
Au_6^-							2.13(2)		2.06(2)	
A 2D	D_{3h}	3.00	2.72	0	0	2.29		2.22		1
B 2D	C_{2v}	3.00	2.75	0.16	309	2.60		2.54		2
C 2D	C_{2v}	2.67	2.70	0.19	367	2.43		2.03		1
D 2D	C_{2v}	2.67	2.69	0.30	580	3.49		3.47		3
Au_7^-							3.46(2)		3.40(3)	
A 2D	C_{2v}	2.86	2.69	0	0	3.46		3.43		2
B 2D	C_s	2.86	2.70	0.04	59	3.32		3.26		1
C 3D	C_{2v}	3.43	2.76	0.47	728	3.57		3.46		3
D 2D	C_{2v}	3.14	2.73	0.54	834	3.43		3.39		3
Au_8^-							2.79(2)		2.73(2)	
A 2D	D_{4h}	3.00	2.69	0	0	2.94		2.88		1
B 2D	C_{2v}	3.50	2.74	0.16	206	3.02		2.98		2
C 2D	C_{2v}	3.00		0.42	541	3.22		3.14		6
D 3D				0.53	683	3.02		2.87		4
E 3D	C_{2v}	3.50	2.74	0.60	774	2.98		2.84		5
F 3D	C_{2v}	4.50	2.82	0.81	1044	2.56		2.45		3
Au_9^-							3.83(2)		3.81(2)	
A 2D	C_{2v}	3.56	2.74	0	0	3.75		3.72		2
B 2D	C_{2v}	3.56	2.74	0.20	220	3.51		3.43		1
C 3D	C_{4v}	3.56	2.74	0.38	420	3.68		3.48		3
D 3D	C_s	4.22	2.80	0.67	740	3.62		3.56		4
Au_{10}^-							3.91(2)		3.89(3)	
A 2D	D_{3h}	3.60	2.73	0	0	3.86		3.84		3
B 2D	D_{2h}	3.80	2.74	0.12	120	2.94		2.91		1
C 2D	C_{2h}			0.33	330	3.14		3.07		2
D 3D	C_{4v}	4.80	2.82	1.27	1230	2.75		2.65		4
Au_{11}^-							3.80(2)		3.76(2)	
A 2D	C_s	3.82	2.74	0	0	3.69		3.64		1
B 2D	C_{2v}	3.64	2.73	0.09	77	3.85		3.82		3
C 2D	D_{2h}	3.64	2.74	0.21	181	3.72		3.68		2
D 3D	C_s	4.00	2.76	0.24	206	3.90		3.81		4
Au_{12}^-							3.06(2)		3.03(2)	
A 2D	D_{3h}	4.00	2.75	0	0	3.24		3.21		1
B 2D	C_{2h}	3.83	2.74	0.32	248	3.25		3.20		2
C 3D	C_{2v}	5.0	2.82	0.54	420	3.10		3.05		3
D 3D	C_{4v}	4.67	2.81	1.33	1029	3.21		3.16		4
Au_{13}^-							3.94(2)		3.91(2)	
A 2D	C_s	3.85	2.74	0	0	4.03		3.98		2
B 3D	C_{2v}	4.92	2.82	0.10	73	3.95		3.93		4
C 2D	C_s	3.85	2.74	0.17	124	3.90		3.84		3
D 2D	D_{6h}	3.69	2.73	0.20	141	4.30		4.26		5
E 2D				0.26	183	3.53		3.51		1
Au_{14}^-							3.00(2)		2.94(2)	
A 2D	C_{2v}	4.00	2.74	0	0	3.66		3.62		5
B 3D	C_{2v}	4.86	2.81	0.10	64	2.93		2.78		2
C 3D	C_s	5.00	2.81	0.23	148	3.25		2.66		3
D 3D	C_{4v}	5.43	2.84	0.27	174	3.33		3.26		4
E 3D				0.31	200	2.68		2.54		1
F 3D				0.35	225	3.76		3.75		6

[a] Shown are the symmetry type (sym), mean coordination number (crd), average bond length (⟨*d*⟩), energy separation of the isomeric structures from the ground-state structures (Δ*E*), expressed both in eV and in K (i.e., in vibrational temperature *T* obtained via the conversion $T = 2\Delta E/3k_B(N-2)$), theoretical and experimental vertical electron detachment energies (VDE^t and VDE^e), theoretical and experimental adiabatic electron detachment energies (ADE^t and ADE^e), and the energy ordering (with 1 denoting the ground state, 2 the first higher-in-energy isomer, etc.) of the corresponding neutral clusters (O^n).

temperature of the clusters was determined to be well below 300 K on the basis of comparison of PES spectra to those

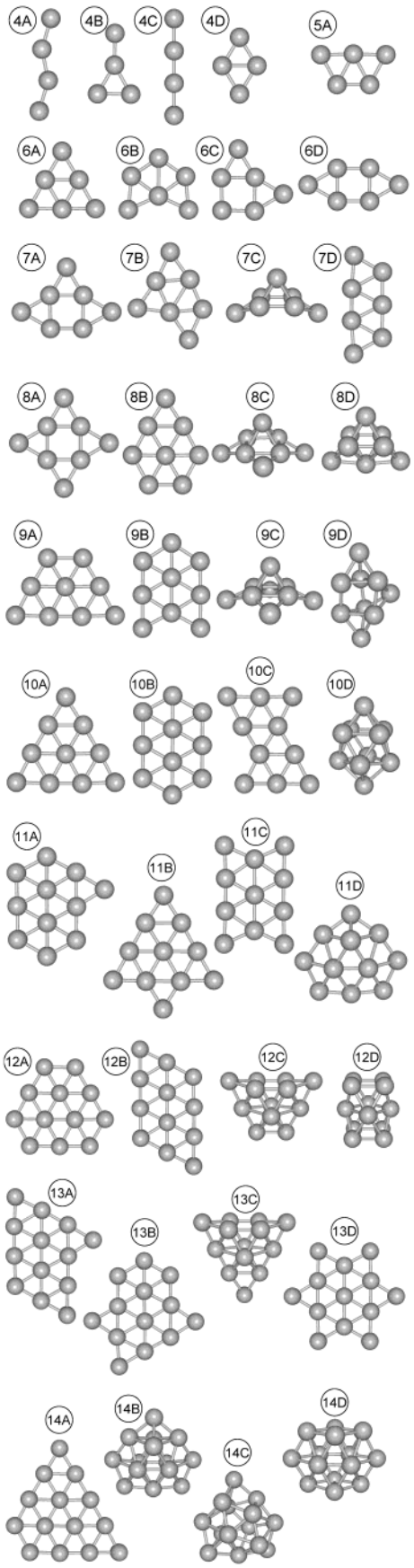

Figure 4. Optimized low-energy structures for Au_N^- clusters with $N = 4-14$. Several isomers are shown for each size, and the ground-state is labeled by "A" in each case. See Table 1 for the corresponding energetic and structural information.

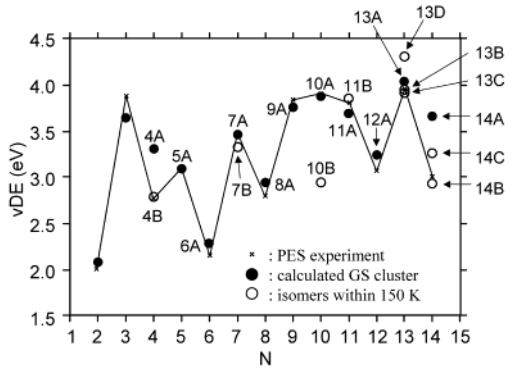

Figure 5. Comparion of theoretical and experimental vertical detachment (VDE) energies. See text for isomers observed experimentally, in particular for $N = 4$ and 10.

derived from DFT simulations, see ref 31), for some cluster sizes isomerization effects have to be considered for a full interpretation of the measured PES data. As will be discussed below, many of the weaker features of the experimental PES data can be attributed to low-lying isomers.

B. Interpretation of the Experimental PES and Assignments of Cluster Structures. In the following we discuss, size-by-size, the measured PES of the Au_N^- cluster anions. On the basis of comparisons between the theoretical VDE values and certain (low-binding-energy) features in the calculated electronic density-of-states (DOS) spectra with the experimental data we assign the most probable clusters structures for the various sizes. To present the theoretical results shown in Figures 6−13, the theoretical DOS spectra were shifted by the self-consistent (cluster-size-dependent) values that place each HOMO level of the spectra to give the negative of the VDE value for the cluster. This procedure is along the lines of the so-called "generalized Koopman's theorem" (GKT),[39] which was shown by us previously, in connection with finite-temperature ab initio molecular dynamics simulations, to work rather well for simple s−p bonded clusters such as aluminum.[31] It should be noted that in comparing of the calculated DOS to the PES data, we focus on the electron binding energies corresponding to the various peaks and not on the relative intensities, because the latter depend on factors that are not included here (mainly the unknown orbital-dependent photodetachment cross-sections).

Au_4^-. The calculations reveal four structures (4A-4D) within an "isomer-coexistence interval" of 0.1 eV (see Figure 4). Because this interval coincides with an estimate of the accuracy of the DFT method for gold clusters (deduced from a comparison between the recent mobility measurements and theoretical calculations[17]), we may assume that members of the tetramer quartet (4A−4D) contribute to the measured PES; the ordering of the cluster isomer (see Table 1) may interchange at finite temperature (due to entropic effects), and in any case it is valid only to within the estimated accuracy indicated above. In the measured PES the first clear peak at 2.75 eV matches the calculated VDE value (2.78 eV) of the isomeric structure 4B, and the very weak features at 2.5 and 3.3 eV are consistent with the calculated DOS of isomer 4D (rhombus; see Figure 6). The DOS of the 4B structure, exhibiting a large HOMO−LUMO gap (see Figure 6), matches best the measured PES spectrum of Au_4^- (Figure 1), and it is likely to be the dominating anion in the experimental Au_4^- cluster distribution.

Au_5^-. Structure 5A is a clear ground state with a separation of 0.3 eV (corresponding to a vibrational temperature of 800 K) from the first isomer 5B. The HOMO level (which is occupied by 2 electrons) is separated by a gap of 0.7 eV from the next deeper lying level (Figure 7), and this agrees reasonably well with the measured gap of about 1 eV. Thus it seems plausible that only the ground-state pentamer anion contributes to the measured PES (Figure 1).

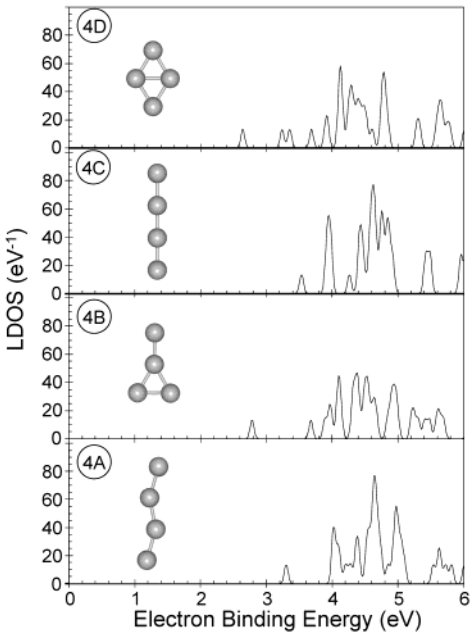

Figure 6. Theoretical generalized Koopman theorem (GKT) -shifted DOS (sum of spin-up and spin-down densities of states) for structures 4A−4D of Au_4^-. In this and subsequent figures, each of the discrete eigenvalues is broadened by a Gaussian with a width $\sigma = 0.05$ eV.

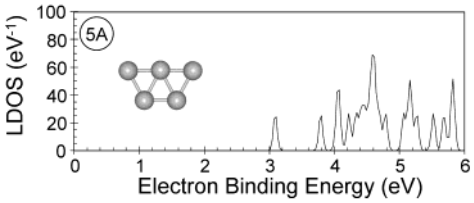

Figure 7. Same as Figure 6 but for structure 5A of Au_5^-.

Au_6^-. The hexamer anion has been studied intensively in the past, and it was shown early on that the measured PES has a very large gap of 2.3 eV between the first two peaks.[2,40] Furthermore, the 2.13 eV VDE peak (agreeing quite well with the theoretical value of 2.29 eV for structure 6A) has been resolved vibrationally with a spacing of 108 cm^{-1},[40] indicating that the structure of the cluster has a high symmetry, which was propsed to be a D_{6h} ring structure.[40] However, the D_{3h} triangular structure 6A has been found to be the clear ground state in scalar-relativistic DFT calculations.[12] The energy difference to the first isomer 6B is 0.16 eV, corresponding to a vibrational temperature of 309 K. Further support for this ground-state structure comes from our ab initio molecular dynamics simulations, where the release of the neutral Au_6 from the anion geometry after electron detachment induces a symmetric vibrational mode of 114 cm^{-1}, compared to the aforementioned experimental result of 108 cm^{-1}. The D_{6h} ring structure can be stabilized only by assuming a high spin state $S = {}^3/_2$, which is 2.02 eV above the $S = {}^1/_2$ D_{3h} ground state 6A. The $S = {}^1/_2$ D_{6h} structure is Jahn−Teller unstable, deforming spontaneously to structure 6D.

The calculated and GKT-shifted DOS of the D_{3h} ground state of Au_6^- is shown in Figure 8 along with the portraits of the LUMO and HOMO wave functions. We observe that the gap

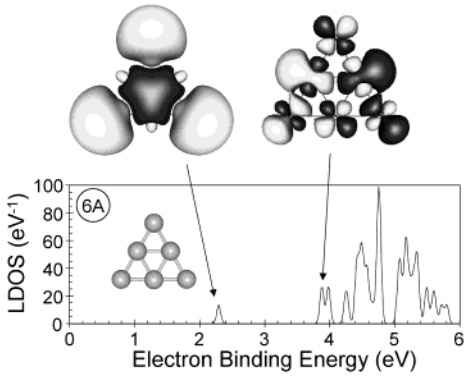

Figure 8. Same as Figure 6 but for structure 6A of Au_6^-. The molecular orbital pictures of the LUMO and HOMO of Au_6 are also shown.

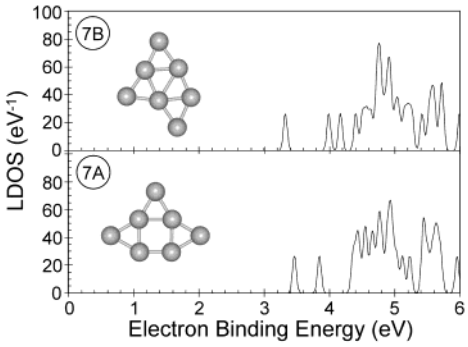

Figure 9. Same as Figure 6 but for structures 7A and 7B of Au_7^-.

separating the first two peaks (HOMO−LUMO gap) in the theoretical DOS is large, 1.58 eV, but still rather small compared to the experimentally determined gap of 2.34 eV. In the special case of spin-doublet anions Au_N^- , with an even N, the first two peaks in the experimental PES are often related to transitions upon electron detachment from the doublet anionic ground state to the neutral spin-singlet and spin-triplet states, and in those cases one is able to determine the aforementioned gap $\Delta E_N^{S-T} = |E_N^S - E_N^T|$ by direct evaluations of total energies of the resulting neutral spin-singlet (E_N^S) and spin-triplet (E_N^T) of the Au_N clusters in the geometry of the anion. For Au_6^- we find that this gap is 1.94 eV, bringing the result closer to the measured value. As shown in the inset in Figure 8, the spatial nature of the LUMO and HOMO states is quite different: although the LUMO state is delocalized and displays significant s-character on the three vertex atoms, the HOMO state shows a higher degree of localization and is clearly composed of atomic d-states.

Au_7^-. The ground state 7A and the first isomer 7B are separated by only 0.04 eV, followed by a clear separation of 0.4 eV from the first three-dimensional isomer 7C. On the basis of our predictions, we conclude that coexistence of the 7A and 7B isomers in the cluster beam (even at low T) is unavoidable. Both structures give theoretical VDE values (3.46 eV for 7A and 3.32 eV for 7B) that match the measured one (3.46 eV). Additionally, we have performed ab initio molecular dynamics simulations over a 4 ps interval at 350 K where several interconversions between structures 7A and 7B occurred. As a result of the dynamics, the low-energy features (up to about 4 eV) in the $T = 0$ DOS (Figure 9) combine into two peaks corresponding to the measured PES in that binding energy range (Figures 1 and 2).

Au_8^-. Both of the two-dimensional structural isomers 8A and 8B are energetically close to each other and should be considered

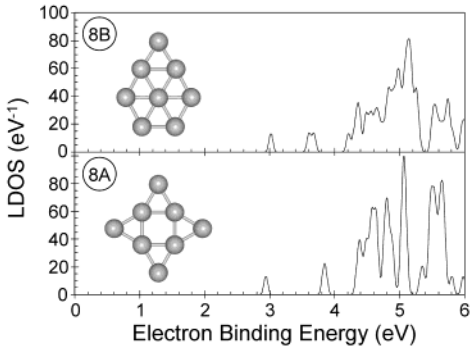

Figure 10. Same as Figure 6 but for structures 8A and 8B of Au_8^-.

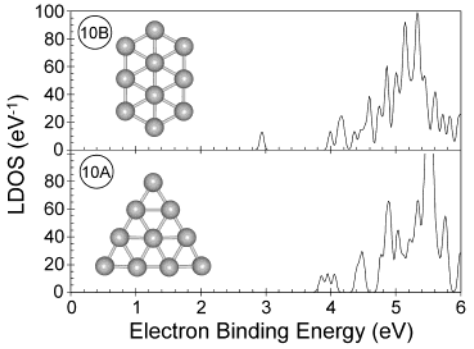

Figure 11. Same as Figure 6 but for structures 10A and 10B of Au_{10}^-.

in interpreting the measured PES data. Indeed, the two features visible in the measured lowest-energy peak could come from the two isomers, with the ground-state 8A giving a VDE of 2.94 in relatively good agreement with the experimental value of 2.79 eV. The calculated VDE (3.02 eV) of isomer 8B is about 0.1 eV higher than that of the 8A isomer and it agrees well with the higher binding energy shoulder of the threshold peak in the PES spectra of Au_8^- (Figures 1 and 2). The two measured higher-energy peaks around 4 eV can also be explained by the corresponding features in the DOS spectra of 8A and 8B (Figure 10).

Au_9^-, Au_{11}^-, and Au_{13}^-. The calculated VDE values of the ground-state structures 9A (3.75 eV), 11A (3.69 eV), and 13A (4.03 eV) agree reasonably well with the experimental values of 3.83, 3.80, and 3.94 eV, respectively. In addition, the calculations predict the existence of several low-lying isomers particularly for $N = 11$ and 13 (two isomers for $N = 11$ and four isomers for $N = 13$ within 200 K from the ground state, measured in terms of the vibrational energy content). We do not attempt to give a detailed interpretation of the experimental PES data here, except to note that the existence of isomeric contributions in the PES cannot be ruled out. This is particularly pertinent for $N = 13$, which is larger than the previously reported critical size ($N = 12$) associated with a 2D−3D transition,[17] where the dimensionality of the clusters in the beam cannot be resolved on the basis of the PES data because our calculated DOS spectra for two- and three-dimensional structures are found to be quite similar (not shown here).

Au_{10}^-. The measured PES spectra of Au_{10}^- differ qualitatively from all the other spectra of even-sized clusters shown here due to the existence of very weak features at 2.9 and 3.5 eV (Figures 1 and 2), as well as the absence of a HOMO−LUMO gap. The first weak peak was previously taken as the VDE value of the cluster.[2] According to our calculations, the planar D_{3h} 10A structure is the ground state, separated by 0.12 eV from the planar D_{2h} isomer. The calculated VDE of 10A is 3.86 eV, in good agreement with the first strong PES peak at 3.91 eV.

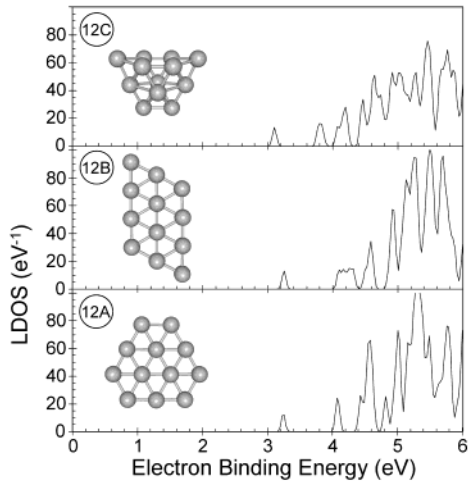

Figure 12. Same as Figure 6 but for structures 12A−12C of Au_{12}^-.

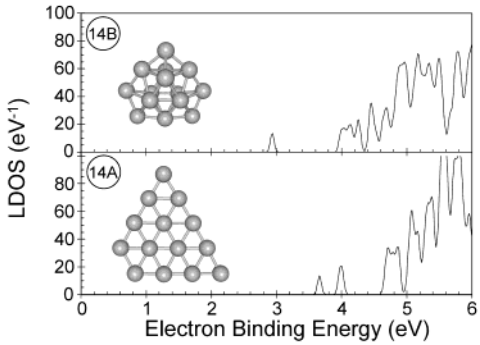

Figure 13. Same as Figure 6 but for structures 14A and 14B of Au_{14}^-.

The VDE of the first isomer, 2.94 eV, matches the first weak PES feature at 2.9 eV.

Au_{12}^-. Our calculations predict the planar D_{3h} structure 12A to be a clear ground state, followed by a planar C_{2h} structure 12B and a 3D C_{2v} structure 12C. The DOS spectra of all these clusters have a clear HOMO−LUMO gap, of the order of 0.8 eV, separating the first two peaks (Figure 12). This agrees well with the experimental PES spectra (Figures 1 and 2), which revealed a HOMO−LUMO gap of about 0.9 eV. On the basis of the comparison between the measured and calculated mobility parameters for clusters 12A and 12C, Kappes et al.[17] concluded that $N = 12$ is the critical size for the 2D-3D transition, namely isomers of both dimensionality are present in the Au_{12}^- anion beam, and clusters with $N > 12$ are three-dimensional. The comparison of our calculated VDE values (12A, 3.24 eV; 12B, 3.25 eV; 12C, 3.10 eV) agree well with the measured value of 3.06 eV. Additionally, the contributions from all these clusters would give a double feature in the first photodetachment peak, as is indeed observed experimentally. Thus, our work gives further support for the conclusion of ref 17 that both planar and 3D structures are present in the beam of Au_{12}^-.

Au_{14}^-. For the cluster anions we found two structures, 14A and 14B, within an energy interval of 0.1 eV, with significantly different DOS features (Figure 13). The experimental data revealed a large HOMO−LUMO gap of 1 eV, which is well reproduced by the three-dimensional cagelike structure 14B (1.05 eV), as well as the calculated singlet−triplet separation (see discussion for $N = 6$ above) $\Delta E_N^{S-T} = 1.07$ eV. Keeping in mind the inherent accuracy of the DFT (of the order of 0.1 eV), as well as the previously reported tendency of DFT to slightly overestimate the stability of planar structures, we assert that the experimental PES for $N = 14$ indicates the predominance of 3D clusters, and the most likely candidate is structure 14B predicted from our calculation. This conclusion is also consistent with that extracted from analysis of ion mobility experiment that above $N = 12$, three-dimensional gold cluster anions become more stable.

C. Energetics and Dimensionality of the Neutral Clusters Au_N, $N = 4-14$. The last column in Table 1, marked by "O^n", indicates the energy ordering of the neutral Au_N clusters as they are relaxed from the corresponding anionic cluster after electron detachment, utilizing the calculated information about the energy difference of various anionic cluster isomers and their adiabatic electron detachment energies. As can be seen, for most cluster sizes the energetic ordering of the neutral clusters does not follow that of the corresponding anions. It is intriguing to note that the planar structures are energetically very competitive with respect to 3D structures also in neutral gold clusters; indeed, only for the largest size considered, Au_{14}, we have found a 3D ground-state structure. Although our theoretical predictions indicate that also neutral gold clusters favor planar structures up to unprecedented large sizes, experimental verification of this result is complicated because the cluster beam experiment usually observes properties of charged clusters. For single positively charged gold clusters Au_N^+ the 2D−3D transition size has been deduced to be $N = 8$ in the ion mobility experiment.[41] Our current theoretical predictions indicate that it should be interesting to study the 2D−3D crossover size experimentally for neutral gold clusters deposited on weak and smooth substrates, such as an ideal graphite surface.

VI. Summary

In this work, well-resolved photoelectron spectra and scalar-relativistic DFT calculations are reported for anionic gold clusters with 1−14 atoms. The combined experimental and theoretical investigation allows us to gain insight into the structural characteristic and growth patterns of the cluster anions and make tentative assignments of the PES features.

In general, we find that the most likely structural candidates for clusters up to $N = 12$ are planar, confirming the findings obtained by Kappes and co-workers[17] from analysis of their mobility experiments. For $N = 13$, a definite structural assignment cannot be done on the basis of the PES data, due to the existence of many low-lying 2D and 3D isomers. For $N = 14$, a 3D cagelike structure has been assigned. Isomeric effects are recognizable in the experimental PES data for several cluster sizes, most notably for $N = 4$, 7, 8, 10, and 12. The 2D-3D transition seems to take place via cagelike structures, but for $N = 13$ the commonly considered icosahedral or cuboctahedral structures are not energetically favorable. This work provides both geometric structural information and characteristics of the electronic structure, which gives the impetus for further theoretical investigations of the physics and chemistry of small gas-phase gold clusters.

Acknowledgment. The experimental work was supported by the National Science Foundation (CHE-9817811) and performed at the W. R. Wiley Environmental Molecular Sciences Laboratory, a national scientific user facility sponsored by DOE's Office of Biological and Environmental Research and located at Pacific Northwest National Laboratory, which is operated for DOE by Battelle under Contract DE-AC06-76RLO 1830. The theoretical work was supported by the U.S. AFOSR and partially (H.H.) by the Academy of Finland. The computa-

tions were performed at NERSC, CA, and in the Center for Computational Materials Science at the Georgia Institute of Technology.

References and Notes

(1) Cox, D. M.; Brickman, R.; Creegan, K.; Kaldor, A. *Z. Phys. D* **1991**, *19*, 353. Cox, D. M.; Brickman, R.; Creegan, K. A. *Mater. Res. Soc. Symp. Proc.* **1991**, *206*, 34.

(2) Taylor, K. J.; Pettiette-Hall, C. L.; Cheshnovsky, C.; Smalley, R. E. *J. Chem. Phys.* **1992,** *96*, 3319.

(3) Handschuh, H.; Gantefor, G.; Bechthold, P. S.; Eberhardt, W. *J. Chem. Phys.* **1994**, *100*, 7093.

(4) Lee, T. H.; Ervin, K. M. *J. Phys. Chem.* **1994**, *98*, 10023.

(5) Haruta, M. *Catal. Today* **1997**, *36*, 153.

(6) Valden, M.; Lai, X.; Goodman, D. W. *Science* **1998**, *281*, 1647.

(7) Garzon, I. L.; Michaelian, K.; Beltrán, M. R.; Posada-Amarillas, A.; Ordejón, P.; Artacho, E.; Sánchez-Portal, D.; Soler, J. M. *Phys. Rev. Lett.* **1988**, *81*, 1600.

(8) Häkkinen, H.; Barnett, R. N.; Landman, U. *Phys. Rev. Lett.* **1999**, *82*, 3264.

(9) Sanchez, A.; Abbet, S.; Heiz, U.; Schneider, W.-D.; Häkkinen, H.; Barnett, R. N.; Landman, U. *J. Phys. Chem. A* **1999**, *103*, 9573.

(10) Bond, G. C.; Thompson, D. T. *Catal. Rev.−Sci. Eng.* **1999**, *41*, 319.

(11) Salisbury, B. E.; Wallace, W. T.; Whetten, R. L. *Chem. Phys.* **2000**, *262*, 131.

(12) Häkkinen, H.; Landman, U. *Phys. Rev. B* **2000**, *62*, R2287.

(13) Grönbeck, H.; Andreoni, W. *Chem. Phys.* **2000**, *262*, 1.

(14) Häkkinen, H.; Landman, U. *J. Am. Chem. Soc.* **2001**, *123*, 9704.

(15) Hagen, J.; Socaciu, L. D.; Elijazyfer, M.; Heiz, U.; Bernhardt, T. M.; Wöste, L. *Phys. Chem. Chem. Phys.* **2002**, *4*, 1707.

(16) Wallace, W. T.; Whetten, R. L. *J. Am. Chem. Soc.* **2002**, *124*, 7499.

(17) Furche, F.; Ahlrichs, R.; Weis, P.; Jacob, C.;. Gilb, S.; Bierweiler, T.; Kappes, M. *J. Chem. Phys.* **2002**, *117*, 6982.

(18) Häkkinen, H.; Moseler, M.; Landman, U. *Phys. Rev. Lett.* **2002**, *89*, 033401. The planar ground-state structures of Au_N^-, $N \leq 13$, were first reported in footnote 28 of this paper. The close similarity of the structures and the isomeric order of the low-lying cluster isomers found in the current work and in ref 17 is encouraging and reassuring in light of the different pseudopotentials, basis sets, and exchange-correlation functionals used in these two independent calculations.

(19) Mills, G.; Gordon, M. S.; Metiu, H. *Chem. Phys. Lett.* **2002**, *359*, 493.

(20) Boyen, H.-G.; Kästle, G.; Weigl, F.; Koslowski, B.; Dietrich, C.; Ziemann, P.; Spatz, J. P.; Riethmüller, S.; Hartmann, C.; Möller, M.; Schmid, G.; Garnier, M. G.; Oelhafen, P. *Science* **2002**, *297*, 1533.

(21) Pyykkö, P.; Runeberg, N. *Angew. Chem. Int. Ed.* **2002**, *41*, 2174.

(22) Li, X.; Kiran, B.; Li, J.; Zhai, H.-J.; Wang, L.-S. Angew. *Chem. Int. Ed.* **2002**, *41*, 4786.

(23) Häkkinen, H.; Abbet, S.; Sanchez, A.; Heiz, U.; Landman, U. *Angew. Chemie Int. Ed.* **2003**, *42*, 1297.

(24) Mills, G.; Gordon, M. S.; Metiu, H. *J. Chem. Phys.* **2003**, *118*, 4198.

(25) Li, J.; Li, X.; Zhai, H.-J.; Wang, L.-S. *Science* **2003**, *299*, 864.

(26) Yoon, B.; Häkkinen, H.; Landman, U. *J. Phys. Chem. A* **2003**, *107*, 4066.

(27) Socaciu, L. D.; Hagen, J.; Bernhardt, T. M.; Wöste, L.; Heiz, U.; Häkkinen, H.; Landman, U. Submitted for publication to *J. Am. Chem. Soc.*

(28) Pyykkö, P. *Chem. Rev.* **1988**, *88*, 563.

(29) Wang, L. S.; Cheng, H. S.; Fan, J. *J. Chem. Phys.* **1995**, *102*, 9480.

(30) Wang, L. S.; Wu, H. In *Advances in Metal and Semiconductor Clusters. IV. Cluster Materials*; Duncan, M. A., Ed.; JAI Press: Greenwich, 1998; pp 299−343.

(31) Akola, J.; Manninen, M.; Häkkinen, H.; Landman, U.; Li, X.; Wang, L. S. *Phys. Rev. B* **1999**, *60*, R11297.

(32) Wang, L. S.; Li, X. In *Proceedings of the International Symposium on Clusters and Nanostructure Interfaces* (Oct. 25−28, 1999, Richmond, VA); Jena, P., Khanna, S. N., Rao, B. K., Ed.; World Scientific: River Edge, NJ, 2000; pp 293−300.

(33) Barnett, R. N.; Landman, U. *Phys. Rev. B* **1993**, *48*, 2081.

(34) Troullier, N.; Martins, J. L. *Phys. Rev. B* **1991**, *43*, 1993.

(35) Perdew, J. P.; Burke, K.; Ernzerhof, M. *Phys. Rev. Lett.* **1996**, *77*, 3865.

(36) Haufler, R. E.; Wang, L. S.; Chibante, L. P. F.; Jin, C.; Conceicao, J.; Chai, Y.; Smalley, R. E. *Chem. Phys. Lett.* **1991**, *179*, 449.

(37) Amrein, A.; Simpson, R.; Hackett, P. *J. Chem. Phys.* **1991**, *94*, 4663.

(38) Bréchignac, C.; Cahuzac, P.; Kebaïli, N.; Leygnier, J. Sarfati, A.; *Phys. Rev. Lett.* **1992**, *68*, 3916.

(39) Tozer, D. J.; Handy, N. C. *J. Chem. Phys.* **1998**, *108*, 2545; *J. Chem. Phys.* **1998**, *109*, 10180.

(40) Taylor, K. J.; Jin, C.; Conceicao, J.; Wang, L.-S.; Cheshnovsky, O.; Johnson, B. R.; Nordlander, P. J.; Smalley, R. E. *J. Chem. Phys.* **1990**, *93*, 7515.

(41) Gilb, S.; Weis, P.; Furche, F.; Ahlrichs, R.; Kappes, M. M. *J. Chem. Phys.* **2002**, *116*, 4094.